The Slope of Form Factors from Lattice QCD

Chia Cheng Chang (張家丞),[1, 2, 3] David Richards,[4] Chris Bouchard,[5] and Kostas Orginos[6, 4]

[1]*Interdisciplinary Theoretical and Mathematical Sciences Program*
(iTHEMS), RIKEN, 2-1 Hirosawa, Wako, Saitama 351-0198, Japan
[2]*Nuclear Science Division, Lawrence Berkeley National Laboratory, Berkeley, CA 94720, USA*
[3]*Department of Physics, University of California, Berkeley, CA 94720, USA*
[4]*Theory Center, Thomas Jefferson National Accelerator Facility, Newport News, VA 23606, USA*
[5]*School of Physics and Astronomy, University of Glasgow, Glasgow G12 8QQ, UK*
[6]*Department of Physics, The College of William & Mary, Williamsburg, VA 23187, USA*

Momentum-space derivatives of matrix elements can be related to their coordinate-space moments through the Fourier transform. We derive these expressions as a function of momentum transfer Q^2 for asymptotic in/out states consisting of a single hadron. We calculate corrections to the finite volume moments by studying the spatial dependence of the lattice correlation functions. This method permits the computation of not only the values of matrix elements at momenta accessible on the lattice, but also the momentum-space derivatives, providing a priori information about the Q^2 dependence of form factors. As a specific application we use the method, at a single lattice spacing and with unphysically heavy quarks, to directly obtain the slope of the isovector form factor at various Q^2, whence the isovector charge radius. The method has potential application in the calculation of any hadronic matrix element with momentum transfer, including those relevant to hadronic weak decays.

I. INTRODUCTION

Answers to some of the deepest mysteries of nature may be uncovered through fundamentally understanding how protons and neutrons, the basic building blocks of our world, interact with the universe. The lattice QCD community has contributed to our understanding of the strength of these interactions by direct calculations of form factors. In this work, we propose a method to directly calculate the slope of these form factors, which shed light on new ways to test our current understanding of the Standard Model.

A. On the radius of the proton

The charged leptons are fundamental (point-like) particles in the Standard Model of particle physics, with identical coupling strengths to the electroweak currents, and only differ in mass between the three generations. This Standard Model paradigm, known as *lepton universality*, is however, in tension with recent experimental observations of the proton charge radius [1]. In particular, measurement from muonic Hydrogen [2] resulted in a 4% smaller proton radius when compared to the CODATA average from 24 transition frequency measurements of atomic Hydrogen [3], in tension at 4 standard deviations. This discrepancy hints at the possibility that the electron and muon may differ fundamentally in ways unaccounted for by the Standard Model. Recently, evidence of possible resolution to the proton radius puzzle was provided by an updated measurement of the 2S-4P transition frequency [4] that is consistent with the muonic Hydrogen measurement. However, a recent update on the 1S-3S transition frequency [5] continues to re-enforce the discrepancy between atomic and muonic experiments.

Electron scattering results continue to exhibit the long standing discrepancy with muonic Hydrogen [6]. Due to the vast number of transition frequencies from Lamb shift measurements, and tension from the electron scattering result, resolution to the charge radius puzzle may still require considerable additional effort from experimentalists. Furthermore, the ratio of semi-leptonic $B \to D^{(*)}\ell\bar{\nu}$ decays to the electron and tau final states is also observed to be in tension with the Standard Model prediction at 4 standard deviations [7], lending evidence that the discrepancy seen in the proton radius may in fact be a result of new physics.

While the measurement of the proton radius is very challenging, its definition is straightforward from a theory stand point. Specifically, the charge radius of the proton $\langle r \rangle$ is defined through the Q^2 derivative of the Sach's form factor $G_E(Q^2)$ evaluated at zero-momentum transfer

$$\left.\frac{\partial G_E(Q^2)}{\partial Q^2}\right|_{Q^2=0} = -\frac{1}{6}\langle r^2 \rangle = \left.\frac{\partial F_1(Q^2)}{\partial Q^2}\right|_{Q^2=0} - \frac{F_2(0)}{4M^2},$$
(1)

where $F_1(Q^2)$ and $F_2(Q^2)$ are the Dirac and Pauli form factors, and M is the proton mass. These form factors are then defined in terms of the matrix elements of the electromagnetic current

$$\langle N(\vec{p}_f) \mid V_\mu(0) \mid N(\vec{p}_i) \rangle =$$
$$\bar{u}(\vec{p}_f)\left[F_1(Q^2)\gamma_\mu + i\sigma_{\mu\nu}q_\nu\frac{F_2(Q^2)}{2M}\right]u(\vec{p}_i) \qquad (2)$$

where $\vec{q} = \vec{p}_f - \vec{p}_i$ is the three-momentum transfer and $Q^2 = (E_f - E_i)^2 - \vec{q}^2$ is the four-momentum transfer entering into eqn. 1. The calculation of both the isovector and isoscalar electromagnetic form factors through the determination of the matrix element defined above is a well-established program in lattice QCD, with extensive

studies aimed at controlling the systematic uncertainties that enter into their evaluation.

Current lattice QCD determinations of the radius, however, remain problematical, because the derivative is extracted from modeling the Q^2 dependence of $F_1(Q^2)$ from calculations at the discrete values of momentum accessible in a finite volume. Indeed, the problems encountered in extracting the charge radius from lattice calculations of the form factor in some respects mirror those in electron-scattering experiments, where the form factor is computed for a descrete, albeit closely spaced, set of finite Q^2, and the need to include dispersive methods in the analysis of the form factors over the values of Q^2 probed in experiment has been emphasised[8]. Thus lattice calculations are susceptible to two major problems: the model dependence that introduces uncontrolled systematic errors, and that the smallest non-zero momentum is too large to perform a controlled extrapolation of the slope at zero-momentum since accessing small momentum in finite volumes requires very large lattices that are prohibitively expensive.

B. On the origin of matter

One of the outstanding mysteries of our universe lies in quest to understand the origin of matter, or more specifically the origin of the matter-antimatter asymmetry that we observe today. There is tantalizing evidence for possible sources of *leptogenesis* recently revealed at the *Tokai-2-Kamioka* (T2K) long-baseline neutrino experiment [9], where CP conservation in the neutrino sector is excluded at 90% confidence. Future long-baseline neutrino experiments including the *Deep Underground Neutrino Experiment* (DUNE), and the detector upgrade to Hyper-Kamiokande (T2HK) aims to provide more precise neutrino oscillation measurements in order to further resolve the neutrino CP-violating phase. Additionally, cost-effective projects such as *CHerenkov detectors In mine PitS* (CHIPS) [10], a water Cherenkov detector designed to be approximately 5 times larger than Super-Kamiokande, is planned with the intention to ultimately run off the DUNE beamline, providing a cost-efficient way to improve knowledge on neutrino parameters including the CP violating phase.

In order to fully benefit from the advances of next generation neutrino experiments, the theoretical description of neutrino scattering must also be made more precise through improving the current determination of the nucleon axial form factor $F_A(Q^2)$. The axial form factor parameterizes the strength in which the weak current couples to the nucleon, and consequently governs the neutrino scattering cross-section off nuclear targets in the regime of quasi-elastic scattering. There is currently a 1–2% uncertainty on the determination of the cross-section [11] that is dominated by the hadronic uncertainty on the axial form factor at small momentum transfer up to approximately 1 GeV [12]. Similar to the

determination of the charge radius, the shape of the form factor is often derived from the model dependent dipole ansatz. Recent progress in lattice QCD has demonstrated control at the percent-level over the axial form factor at zero-momentum transfer [13]. The method introduced in this paper is extensible to calculations of the slope at non-zero momentum transfer and paves a way for controlling the full momentum dependence of the form factor at the same level of precision.

C. Overview

The remainder of the paper is laid out as follows. In the next section, we introduce moment methods in which time-sliced correlation functions are weighted by moments of a spatial coordinate, and demonstrate how these methods enable the momentum-dependent slope of form factors to be directly computed at the momenta allowed on the lattice. We describe previous applications of the method, and then describe how these methods can be used to determine the slope of the nucleon electromagnetic form factors at $Q^2 = 0$, and hence the charge radius of the nucleon. We concluded the section by describing our analysis method, emphasising in particular the need to allow for excited-state contributions to the correlation functions, and the anticipated finite-volume behaviour.

In Section III, we present the application of the method to the isovector charge radius of the nucleon. We begin by describing the parameters of the ensembles used in our calculation, emphasising the need to understand the dependence of the results on the spatial volume of our lattices. We present results for the charge radius for several separations between the nucleon source and nucleon sink, demonstrating the need to include the contribution of excited nucleon states in our fitting procedure. The calculation is performed at unphysically large values of the pion mass, and at a relatively coarse lattice spacing. We conclude with an program of future work, and of other applications, including to the determination of the axial-vector charge radius.

We emphasise that the aim of this paper is not to provide a direct calculation of the charge radius that can confront experiment, but rather to present a method that can address one of the main systematic uncertainties that plague present calculations.

II. MOMENTS OF CORRELATION FUNCTIONS

Position-space moment methods was first introduced to calculate the slope of the Isgur-Wise function $\xi(w)$ at zero-recoil, in order to interpret experimental results near zero-recoil for $B \to D$ semi-leptonic decays [14], and later adapted to calculate the slope of the energy-momentum tensor form factor, yielding the angular momentum contribution to the spin of the nucleon [15, 16]. Recently,

there is revitalized interest in applying moment methods to calculate the hadronic vacuum polarization [17, 18], and efforts to directly determine the anomalous magnetic moment of the nucleon and radii in nuclear physics [19]. In parallel, momentum-space derivative methods are also being explored to access similar nucleon structure calculations such as the anomalous magnetic moment and various nucleon radii [20, 21]. In this work, we present a coordinate-space method that directly calculates the slope of single particle form factors with respect to the squared momentum-transfer at any lattice accessible momenta.

A. Charge radius spinor algebra

Here we present the spinor algebra necessary to obtain the derivative of the Dirac form factor $F_1(Q^2)$ from the derivative of the electromagnetic matrix element. We work explicitly in the Degrand-Rossi basis defined as

$$
\gamma_1 = \begin{pmatrix} 0 & 0 & 0 & i \\ 0 & 0 & i & 0 \\ 0 & -i & 0 & 0 \\ -i & 0 & 0 & 0 \end{pmatrix} \quad \gamma_2 = \begin{pmatrix} 0 & 0 & 0 & -1 \\ 0 & 0 & 1 & 0 \\ 0 & 1 & 0 & 0 \\ -1 & 0 & 0 & 0 \end{pmatrix}
$$

$$
\gamma_3 = \begin{pmatrix} 0 & 0 & i & 0 \\ 0 & 0 & 0 & -i \\ -i & 0 & 0 & 0 \\ 0 & i & 0 & 0 \end{pmatrix} \quad \gamma_4 = \begin{pmatrix} 0 & 0 & 1 & 0 \\ 0 & 0 & 0 & 1 \\ 1 & 0 & 0 & 0 \\ 0 & 1 & 0 & 0 \end{pmatrix}
\tag{3}
$$

and define momentum of the spinors to point in the z-direction without loss of generality. Additionally we restrict ourselves to aligning the spin to be (anti-)parallel with momentum, yielding the following positive- and negative-helicity particle spinors,

$$
u_+(p) = \begin{pmatrix} \sqrt{E-p} \\ 0 \\ \sqrt{E+p} \\ 0 \end{pmatrix} \quad u_-(p) = \begin{pmatrix} 0 \\ \sqrt{E+p} \\ 0 \\ \sqrt{E-p} \end{pmatrix}.
\tag{4}
$$

Next, we explicitly work out the spinor contraction for the V_4 current in the rest frame of the final state nucleon such that $\vec{p}_f = 0$ and $\vec{p}_i = -q_3 \equiv k$ as shown in Fig. 1. Following Eq. (2),

$$
\langle N(\vec{p}_f)|V_4(q^2)|N(\vec{p}_i)\rangle
$$
$$
= \bar{u}(\vec{p}_f) \left[F_1(Q^2)\gamma_4 + i\sigma_{43}q_3 \frac{F_2(Q^2)}{2M} \right] u(\vec{p}_i).
\tag{5}
$$

In the case of a $u_\pm \to u_\mp$ transition, the matrix element vanishes. However, if helicity is conserved, then Eq. (5) simplifies to,

$$
\langle N(0)|V_4|N(k)\rangle = F_1\sqrt{M}\left(\sqrt{E+k} + \sqrt{E-k} \right),
\tag{6}
$$

where M is the rest mass of the nucleon. Taking the zero-momentum transfer limit after the 3-momentum-squared
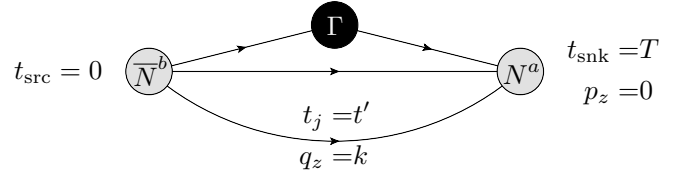

FIG. 1. Kinematics of the three-point correlator with baryon initial and final states. We work in the rest frame of the final hadron. The diagram for semi-leptonic decays of mesons involves only one spectator quark, but involves the same kinematics. Change a and b to say src and snk.

derivative yields,

$$
\frac{\partial}{\partial k^2}\langle N(0)|V_4|N(k)\rangle\bigg|_{k=0}
$$
$$
= \frac{\partial F_1}{\partial k^2}\sqrt{M}\left(\sqrt{E+k} + \sqrt{E-k} \right)\bigg|_{k=0}
$$
$$
+ F_1\frac{\sqrt{M}}{4k}\left(\frac{1}{\sqrt{E+k}} - \frac{1}{\sqrt{E-k}} \right)\bigg|_{k=0}
$$
$$
= 2M\frac{\partial F_1}{\partial k^2},
\tag{7}
$$

yielding directly the derivative of the Dirac form factor at zero-momentum transfer. Following Eq. (5), V_1 and V_2 accesses matrix elements that are proportional to kF_2 but vanish in the zero-momentum transfer limit, while the k^2-derivative of V_3 diverges.

B. Formalism

Some more self-plagiarism.

1. Three-point correlation function

Given a three-point correlation function with the initial state at rest, and current insertion with three-momentum k, where k points in the z-direction without loss of generality, as shown in Fig. 1, the three-momentum-projected three-point has the general form,

$$
C^{3\text{pt}}(t,t') = \sum_{\vec{x},\vec{x}'} \left\langle N^{\text{snk}}_{t,\vec{x}} \Gamma_{t',\vec{x}'} \overline{N}^{\text{src}}_{0,\vec{0}} \right\rangle e^{-ikx'_z},
\tag{8}
$$

translational invariance allows us to shift the source to the origin $\vec{x}_{\text{src}} = 0$ and the sink to $\vec{x} \equiv \vec{x}_{\text{snk}} - \vec{x}_{\text{src}}$. Since the sink has zero three-momentum, the only momentum dependence left is at the current insertion. The operators N^{src} and N^{snk} are the source and sink interpolation operators respectively, allowing for different choices of the nucleon interpolating operator [22, 23] and operator smearing profiles. The operator Γ is a generic current insertion at position $\vec{x}' \equiv \vec{x}_J - \vec{x}_{\text{src}}$.

The derivative of the three-point correlator with respect to k^2 follows,

$$C'_{3\text{pt}}(t,t') = \sum_{\vec{x},\vec{x}'} \frac{-x'_z}{2k} \sin\left(kx'_z\right) \left\langle N^{\text{snk}}_{t,\vec{x}} \Gamma_{t',\vec{x}'} \overline{N}^{\text{src}}_{0,\vec{0}} \right\rangle, \quad (9)$$

where in Eq. (9), the cosine component vanishes due to symmetry. In the limit of zero momentum, the $k^2 \to 0$ limit of the integrand is given by L'Hôpital's rule,

$$\lim_{k^2 \to 0} C'_{3\text{pt}}(t,t') = \sum_{\vec{x},\vec{x}'} \frac{-x'^2_z}{2} \left\langle N^{\text{snk}}_{t,\vec{x}} \Gamma_{t',\vec{x}'} \overline{N}^{\text{src}}_{0,\vec{0}} \right\rangle. \quad (10)$$

While it is tempting to think of Eq. (10) as having an x'^2_z moment, it is clear from Eq. (9), that a single derivative contributes only a single factor of x'_z. The second factor of x'_z only appears in the $k^2 \to 0$ limit and should not be thought as a position-space moment resulting from a momentum-space derivative.

2. Two-point correlation function

Analogously, given a two-point correlator with three-momentum k in the z-direction,

$$C_{2\text{pt}}(t) = \sum_{\vec{x}} \left\langle N^{\text{snk}}_{t,\vec{x}} \overline{N}^{\text{src}}_{0,\vec{0}} \right\rangle e^{-ikx_z}, \quad (11)$$

the derivative of the two-point correlator with respect to k^2 follows,

$$C'_{2\text{pt}}(t) = \sum_{\vec{x}} \frac{-x_z}{2k} \sin\left(kx_z\right) \left\langle N^{\text{snk}}_{t,\vec{x}} \overline{N}^{\text{src}}_{0,\vec{0}} \right\rangle. \quad (12)$$

Analogous to the moment of the three-point correlator, the cosine contribution vanishes due to symmetry. Consequently, in the zero-momentum limit,

$$\lim_{k^2 \to 0} C'_{2\text{pt}}(t) = \sum_{\vec{x}} \frac{-x^2_z}{2} \left\langle N^b_{t,\vec{x}} \overline{N}^b_{0,\vec{0}} \right\rangle. \quad (13)$$

The construction of the moment of the two-point correlator is similar to the moment of the three-point correlator with the exception that the moment now depends on the final state position x_z instead of the current insertion position x'_z. In both cases, the spatial dependence for all momenta are even, resulting in a non-vanishing correlator under the Fourier transform, explicitly circumventing the concern raised in Ref [24]. Given prior computational investment in generating the propagators and sequential propagators, the generation of the moments of correlators only differ during the Fourier transform, and therefore require negligible additional computing time to construct.

C. Interpretation

1. Three-point correlation function

In the rest frame of the final state hadron, the spectral decomposition of the three-point correlation function in

Eq. (8) is

$$C_{3\text{pt}}(t,t') = \sum_{n,m} \frac{Z^{\dagger\text{snk}}_m(0)\Gamma_{mn}(k^2)Z^{\text{src}}_n(k^2)}{4E_m(0)E_n(k^2)}$$
$$\times e^{-E_m(0)(t-t')} e^{-E_n(k^2)t'}. \quad (14)$$

The time dependence involves the source-sink separation $t \equiv t^{\text{snk}} - t^{\text{src}}$ and the insertion-sink separation $t' \equiv t^{\text{ins}} - t^{\text{src}}$. The parameters $E_n(k^2)$ infer the n-th state energy of the hadron with momentum k^2, $\Gamma_{mn}(k^2)$ infers the $n \to m$-th state matrix element, and $Z^{\text{src(snk)}}_{n(m)}$ infers the overlap factor at the source and sink, which in general is different and depends on the interpolating operator and smearing profile used. On the lattice, the path integral is performed under a Wick rotation, yielding the exponential time dependence. At large time separations, the ground state signal exponentially dominates the correlation function.

Taking the k^2 derivative of Eq. (14) yields the spectral decomposition of the correlator generated by Eqs. (9, 10),

$$C'_{3\text{pt}}(t,t') = \sum_{m,n} C^{mn}_{3\text{pt}}(t,t') \left[\frac{\Gamma'_{mn}(k^2)}{\Gamma_{mn}(k^2)} \right.$$
$$\left. + \frac{Z'^{\text{src}}_n(k^2)}{Z^{\text{src}}_n(k^2)} - \frac{1}{2E^2_n(k^2)} - \frac{t'}{2E_n(k^2)} \right], \quad (15)$$

where $C^{mn}_{3\text{pt}}$ is the $n \to m$-th state contribution of Eq. (14) and Γ' is the k^2 derivative of the matrix element Γ. Extracting Γ' is the main goal of this paper. An additional consequence is the dependence on Z'^{src}, the k^2 derivative of the source overlap factor, which can be analogously extracted from the derivative of the two-point correlator. Here we note that in the rest-frame of the final hadron, only Z'^{src} survives, while any dependence on Z'^{snk} explicitly vanishes, where the source and sink operators here apply to the three-point correlation function, and in general may be different from the operators used in the two-point correlator in the following discussion.

2. Two-point correlation function

The spectral decomposition of the two-point correlation function constructed from Eq. (11) is,

$$C_{2\text{pt}}(t) = \sum_m \frac{Z^{\dagger\text{snk}}_m(k^2)Z^{\text{src}}_m(k^2)}{2E_m(k^2)} e^{-E_m(k^2)t} \quad (16)$$

where on a given lattice, $t \equiv t^{\text{snk}} - t^{\text{src}}$ is the same source-sink separation t in Eqs. (14, 15). While in general, the source and sink operators may be different from the three-point correlation function, at least one of the operators has to be the same as the three-point source operator in order to disentangle Γ' from Z'^{src} from Eq. (15).

Taking the k^2 derivative of Eq. (16) yields,

$$C'_{2\text{pt}}(t) = \sum_m C^m_{2\text{pt}}(t) \left[\frac{Z'^{\dagger\text{snk}}_m(k^2)}{Z^{\dagger\text{snk}}_m(k^2)} + \frac{Z'^{\text{src}}_m(k^2)}{Z^{\text{src}}_m(k^2)} \right.$$

$$-\frac{1}{2E_m^2(k^2)} - \frac{t}{2E_m(k^2)}\Bigg], \qquad (17)$$

where Z' is the k^2 derivative of the overlap factors. In particular, $Z' = 0$ for point sources and sinks since a Dirac delta function provides equal support for all momenta.

3. 4-momentum derivatives

The lattice correlation functions and the corresponding spectral decomposition is computed by directly taking the 3-momentum derivative. In general however, the radius of a hadron, or more generally the form factor, depends on the 4-momentum transfer squared $Q^2 = -q^2$ where

$$-q \equiv \begin{pmatrix} E_n(k^2) - M_m \\ 0 \\ 0 \\ k \end{pmatrix}, \qquad (18)$$

which we again, assume that the final state hadron is at rest, such that $M_m = E_m(0)$. As a result, the Q^2 derivative of the matrix element is related to the k^2 derivative through the chain rule,

$$\frac{\partial}{\partial k^2}\Gamma_{mn} = \frac{\partial Q^2}{\partial k^2}\frac{\partial}{\partial Q^2}\Gamma_{mn} = \frac{M_m}{\sqrt{M_n^2 + k^2}}\frac{\partial}{\partial Q^2}\Gamma_{mn}, \quad (19)$$

where M_n and M_m is respectively the rest mass of the initial and final state hadron.

D. Reparameterization

Dependence on the inverse of the matrix elements and overlap factors may lead to numerical instability especially when a large number of excited states are included in the fit ansatz. This is due to the fact that *a priori* the sign of the excited state parameters are unknown, and values close to zero may be sampled. In order to improve numerical stability, the following reparameterizations are suggested.

For the two- and three-point correlation function the factors of of E are absorbed into the definition of Z and Γ,

$$C_{2\text{pt}}(t) = \sum_m z_m^{\dagger\text{snk}}(k^2) z_m^{\text{src}}(k^2) e^{-E_m(k^2)t}, \qquad (20)$$

$$C_{3\text{pt}}(t,t') = \sum_{m,n} z^{\dagger\text{snk}}(0) g_{mn}(k^2) z_n^{\text{src}}(k^2)$$
$$\times e^{-E_m(0)(t-t')} e^{-E_n(k^2)t'}, \qquad (21)$$

such that

$$z_n \equiv \frac{Z_n(k^2)}{\sqrt{2E_n(k^2)}}, \qquad (22)$$

$$g_{mn} \equiv \frac{\Gamma_{mn}(k^2)}{2\sqrt{E_m(0)E_n(k^2)}}. \qquad (23)$$

Parameters from the derivative correlation function may be inferred using,

$$C'_{2\text{pt}}(t) = \sum_m C_{2\text{pt}}^m(t) \Bigg[z_m'^{\dagger\text{snk}}(k^2) + z_m'^{\text{src}}(k^2)$$
$$-\frac{1}{2E_m^2(k^2)} - \frac{t}{2E_m(k^2)}\Bigg], \qquad (24)$$

$$C'_{3\text{pt}}(t,t') = C_{3\text{pt}}^{mn}(t,t') \Bigg[g'_{mn}(k^2) + z_n'^{\text{src}}(k^2)$$
$$-\frac{1}{2E_m^2(k^2)} - \frac{t'}{2E_m(k^2)}\Bigg], \qquad (25)$$

where

$$z_n'^{\text{src(snk)}} \equiv \frac{Z_n'^{\text{src(snk)}}(k^2)}{z_n^{\text{src(snk)}}(k^2)\sqrt{2E_n(k^2)}}, \qquad (26)$$

$$g'_{mn} \equiv \frac{\Gamma'_{mn}}{2g_{mn}\sqrt{E_m(0)E_n(k^2)}}. \qquad (27)$$

The Dirac radius contribution of Eq. (1), can therefore, be calculated directly from lattice QCD

$$-\frac{1}{6}\langle r_{\text{Dirac}}^2 \rangle = \frac{\partial F_1(Q^2)}{\partial Q^2}\Bigg|_{Q^2=0}$$
$$= g_{00}g'_{00}. \qquad (28)$$

E. Valence finite volume correction

The valence finite volume corrections results from 1) truncating the spatial moment at $z = L/2$, and applying the incorrect spatial moment between $[0, L/2]$ for periodic images coming from 2) $z \geq L$ and 3) $z \leq -L$. In this section we discuss how to correct for valence finite volume effects which arise from both contributions. In the following derivation, we make the assumption that past $L/2$, only the salient contribution comes from the ground state.

Before discussing the volume corrections, we first discuss the various contributions to the three-point correlation function in the spatial direction. In Fig. 2 (Left), we plot the correlator as a function of current insertion position z' after projecting to zero-momentum in x', y', and t'. We then perform a 3-state fit from $z' = [4, 16]$ and extract the ground state and first excited-state parameters. Note that the correlator is symmetric by construction from averaging with the parity inverted counterpart, and in conjunction, a symmetric fit function is also employed. We observe that at ~ 400 MeV pion masses, the propagating scale in the spatial-direction for the three-point correlator is ~ 820 MeV, corresponding to the mass of the rho-meson (~ 770 MeV) what is the rho at 400 MeV? with one unit of momentum (~ 120 MeV) for a total energy of ~ 780 MeV update if rho mass changes? This
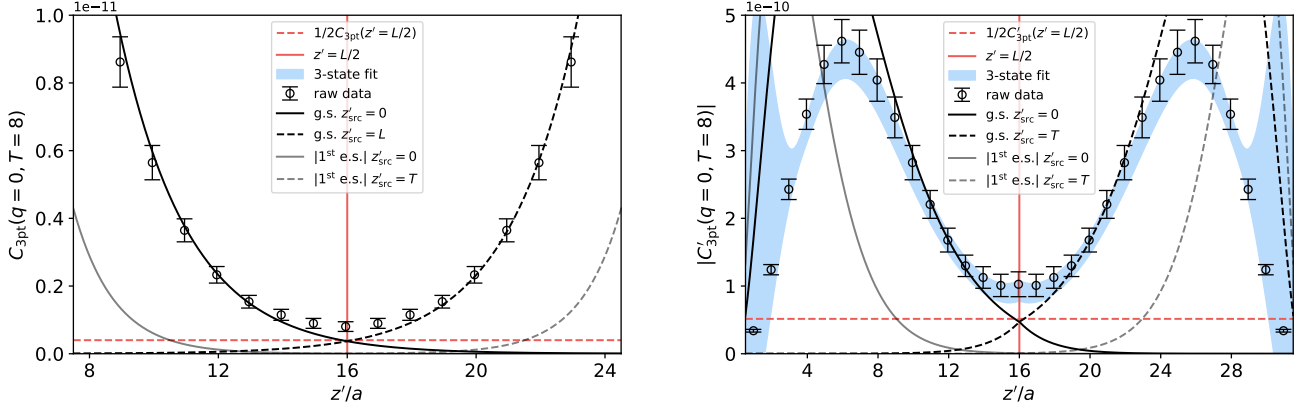
FIG. 2. (Left) blah blah..

is consistent with expectation since the vector current yields a vector-meson propagating state, and the temporal direction has anti-periodic boundary conditions with length $T = 96$. Additionally, we observe that beyond $L/2$, the correlation function is dominated by the ground state.

In Fig. 2 (Right), we take the results from Fig. 2 (Left) and construct the zero-momentum moment correlation function. As expected, the spatial moment pushes the dominant contribution of the correlation function to larger values of z' (maximally around $z' \sim 7$ instead of at zero). Additionally, since the spatial moment is itself not periodic and truncated at $z' = L/2$, the moment correlation function deviates from Eq. (10). We observe again however, that only the ground-state needs to be considered, since the first-excited state has insignificant contribution for $z' \geq L/2$.

The positive-correction to truncating the spatial moment at $L/2$ is given as follows.

$$\delta_1|_{k \neq 0} = 2 \int_{L/2}^{\infty} \frac{-iA_0}{2k} z(-i\sin(kz)) e^{-E_0 z} dz \qquad (29)$$

$$= \frac{-A_0 e^{-E_0 L/2}}{2(E_0^2 + k^2)^2} \left[E_0^2 L + k^2 L + 4E_0 \right] \cos(kL/2) \qquad (30)$$

$$\lim_{k \to 0} \delta_I = -A_0 \left(\frac{L^2}{4E_0} + \frac{L}{E_0^2} + \frac{2}{E_0^3} \right) e^{-E_0 L/2}. \qquad (31)$$

The factor of 2 in Eq. (29) arises from performing a symmetric integral around the origin, E_0 is the ground state energy, A_0 is the ground-state coefficient of the correlation function, and $k = \frac{2n\pi}{L}$. Taking the zero-momentum limit requires keeping the $\sin(kL/2)$ contribution of Eq. (30), which otherwise vanishes at non-zero momentum from symmetry.

The negative-correction from applying the spatial mo-

ment to periodic images from $z' \geq L$ is derived below.

$$\delta_2|_{k \neq 0} = 2 \int_0^{L/2} \frac{-iA_0}{2k} z(-i\sin(kz)) \sum_{n=1}^{\infty} e^{E_0(z-nL)} dz \qquad (32)$$

$$\qquad (33)$$

$$\lim_{k \to 0} \delta_2 = \frac{A_0 e^{-E_0 L}}{1 - e^{-E_0 L}} \left[e^{E_0 L/2} \left(\frac{L^2}{4E_0} - \frac{L}{E_0^2} + \frac{2}{E_0^3} \right) - \frac{2}{E_0^3} \right]. \qquad (34)$$

Finally, the negative-correction from applying the spatial moment to periodic images from $z' \leq -L$ is,

$$\delta_3|_{k \neq 0} = 2 \int_0^{L/2} \frac{-iA_0}{2k} z(-i\sin(kz)) \sum_{n=1}^{\infty} e^{-E_0(z+nL)} dz \qquad (35)$$

$$\qquad (36)$$

$$\lim_{k \to 0} \delta_3 = \frac{A_0 e^{-E_0 L}}{1 - e^{-E_0 L}} \left[e^{-E_0 L/2} \left(\frac{L^2}{4E_0} + \frac{L}{E_0^2} + \frac{2}{E_0^3} \right) - \frac{2}{E_0^3} \right]. \qquad (37)$$

III. CHARGE RADIUS OF THE PROTON

A. Computational Details

To demonstrate the efficacy of this approach, we perform the calculation on the Jefferson Lab isotropic clover lattices, with two light (up/down) quark flavors, and a strange quark, that is fixed to its physical value, and at two different volumes. Since an important aim of this paper is to investigate the dependence of the results on the spatial volume of the box in which the calculation is performed, we work at relatively coarse lattice spacing of approximately 0.12fm; in contrast to the preliminary results presented in ref. [25], these ensembles have

Label	Size	β	a[fm]	m_π[MeV]	$m_\pi L$	$N_{\rm cfg}$	$N_{\rm src}$
l3296	$32^3 \times 96$	6.1	0.12	400	7.7	196	2
l4896	$48^3 \times 96$	6.1	0.12	400	11.5	98	2

TABLE I. The details of the ensembles used in the calculation, denoted by the labels in the first column. The lattice spacing is obtained using ω_0 to set the scale, while the final column lists the number of time sources used for the two-point and three-point functions on each configuration.

larger spatial volume, and are not replicated along the z-direction. Properties of the ensembles are summarized in Table I.

The three-point correlation functions are constructed using a 'sequential propagator' with sink-locations at $T = \{8, 10\}$.

B. Analysis strategy

For the following analysis, the ground state parameters are extracted from a simultaneous fit to $C_{\rm 2pt}(t)$, $C'_{\rm 2pt}(t)$, $C_{\rm 3pt}(t,t')$, and $C'_{\rm 3pt}(t,t')$ for both $k = 0$ and $2\pi/L$. Parametric inference is performed under the Bayesian framework and implemented by the Python library `lsqfit` [26]. Robustness of the fit is demonstrated by performing a sensitivity analysis under varying fit re-

gions for all 8 correlation functions, and the number of states in the fit ansatz. Due to having relatively low statistics, the fit region is restricted to contain a smaller number of degrees-of-freedom to avoid systematic errors when inverting the covariance matrix. Additionally, we check that the ground state energy and the overlap factors satisfy the dispersion relation over different momenta.

C. Correlator analysis

1. Prior selection

2. Fit region

For example, the preferred fit on the l3296 ensemble contains 36 data points from 8 correlation functions, while the two-state fit ansatz contains a total of 24 parameters. A fit with more than two states will contain more parameters than data points, and prior information is required.

3. Sensitivity analysis

IV. CONCLUSIONS AND OUTLOOK

This is a great paper. Please publish. Thanks.

[1] C. E. Carlson, Prog. Part. Nucl. Phys. **82**, 59 (2015), arXiv:1502.05314 [hep-ph].

[2] R. Pohl, A. Antognini, F. Nez, F. D. Amaro, F. Biraben, J. M. R. Cardoso, D. S. Covita, A. Dax, S. Dhawan, L. M. P. Fernandes, A. Giesen, T. Graf, T. W. Hänsch, P. Indelicato, L. Julien, C.-Y. Kao, P. Knowles, E.-O. Le Bigot, Y.-W. Liu, J. M. Lopes, L. Ludhova, C. M. B. Monteiro, F. Mulhauser, T. Nebel, P. Rabinowitz, J. M. F. dos Santos, L. A. Schaller, K. Schuhmann, C. Schwob, D. Taqqu, J. F. C. A. Veloso, and F. Kottmann, Nature **466**, 213 EP (2010).

[3] P. J. Mohr, B. N. Taylor, and D. B. Newell, Rev. Mod. Phys. **80**, 633 (2008).

[4] A. Beyer, L. Maisenbacher, A. Matveev, R. Pohl, K. Khabarova, A. Grinin, T. Lamour, D. C. Yost, T. W. Hänsch, N. Kolachevsky, and T. Udem, Science **358**, 79 (2017), http://science.sciencemag.org/content/358/6359/79.full.pdf.

[5] H. Fleurbaey, *Frequency metrology of the 1S-3S transition of hydrogen: contribution to the proton charge radius puzzle*, Theses, Université Pierre et Marie Curie (UPMC) (2017).

[6] I. Sick, (2018), arXiv:1801.01746 [nucl-ex].

[7] G. Ciezarek, M. Franco Sevilla, B. Hamilton, R. Kowalewski, T. Kuhr, V. Lüth, and Y. Sato, Nature **546**, 227 (2017), arXiv:1703.01766 [hep-ex].

[8] J. M. Alarcón and C. Weiss, (2018), arXiv:1803.09748 [hep-ph].

[9] K. Abe et al. (T2K), Phys. Rev. Lett. **118**, 151801 (2017), arXiv:1701.00432 [hep-ex].

[10] P. Adamson et al., in *Proceedings, 2013 Community Summer Study on the Future of U.S. Particle Physics: Snowmass on the Mississippi (CSS2013): Minneapolis, MN, USA, July 29-August 6, 2013* (2013) arXiv:1307.5918 [physics.ins-det].

[11] C. Adams et al. (LBNE), (2013), arXiv:1307.7335 [hep-ex].

[12] M. Day and K. S. McFarland, Phys. Rev. **D86**, 053003 (2012), arXiv:1206.6745 [hep-ph].

[13] C. C. Chang et al., in *35th International Symposium on Lattice Field Theory (Lattice 2017) Granada, Spain, June 18-24, 2017* (2017) arXiv:1710.06523 [hep-lat].

[14] L. Lellouch, J. Nieves, C. T. Sachrajda, N. Stella, H. Wittig, G. Martinelli, and D. G. Richards (UKQCD), Nucl. Phys. **B444**, 401 (1995), arXiv:hep-lat/9410013 [hep-lat].

[15] N. Mathur, S. J. Dong, K. F. Liu, L. Mankiewicz, and N. C. Mukhopadhyay, Phys. Rev. **D62**, 114504 (2000), arXiv:hep-ph/9912289 [hep-ph].

[16] V. Gadiyak, X.-d. Ji, and C.-w. Jung, Phys. Rev. **D65**, 094510 (2002), arXiv:hep-lat/0112040 [hep-lat].

[17] B. Chakraborty, C. T. H. Davies, P. G. de Oliveira, J. Koponen, and G. P. Lepage, (2016), arXiv:1601.03071 [hep-lat].
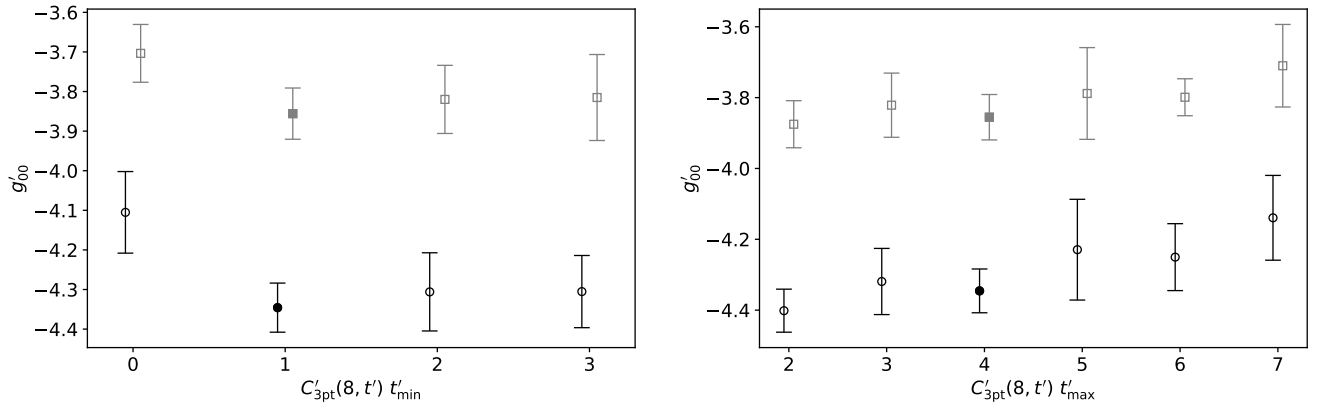
FIG. 3. (Left) Stability plot and (Right) Q-value for the matrix element derivative under varying t_{min} of the two-point correlation function, and n-states. The preferred fit is shown by the solid green points.

[18] T. Blum *et al.* (RBC/UKQCD), JHEP **04**, 063 (2016), arXiv:1602.01767 [hep-lat].

[19] C. Alexandrou, M. Constantinou, G. Koutsou, K. Ottnad, and M. Petschlies (ETM), (2016), arXiv:1605.07327 [hep-lat].

[20] G. M. de Divitiis, R. Petronzio, and N. Tantalo, Phys. Lett. **B718**, 589 (2012), arXiv:1208.5914 [hep-lat].

[21] B. C. Tiburzi, Phys. Rev. **D90**, 054508 (2014), arXiv:1407.4059 [hep-lat].

[22] S. Basak, R. Edwards, G. T. Fleming, U. M. Heller, C. Morningstar, D. Richards, I. Sato, and S. J. Wallace (Lattice Hadron Physics (LHPC)), Phys. Rev. **D72**, 074501 (2005), arXiv:hep-lat/0508018 [hep-lat].

[23] S. Basak, R. G. Edwards, G. T. Fleming, K. J. Juge, A. Lichtl, C. Morningstar, D. G. Richards, I. Sato, and S. J. Wallace, Phys. Rev. **D76**, 074504 (2007), arXiv:0709.0008 [hep-lat].

[24] W. Wilcox, Phys. Rev. **D66**, 017502 (2002), arXiv:hep-lat/0204024 [hep-lat].

[25] C. Bouchard, C. C. Chang, K. Orginos, and D. Richards, *Proceedings, 34th International Symposium on Lattice Field Theory (Lattice 2016): Southampton, UK, July 24-30, 2016*, PoS **LATTICE2016**, 170 (2016), arXiv:1610.02354 [hep-lat].

[26] G. P. Lepage, "`lsqfit` v9.3," (2018).

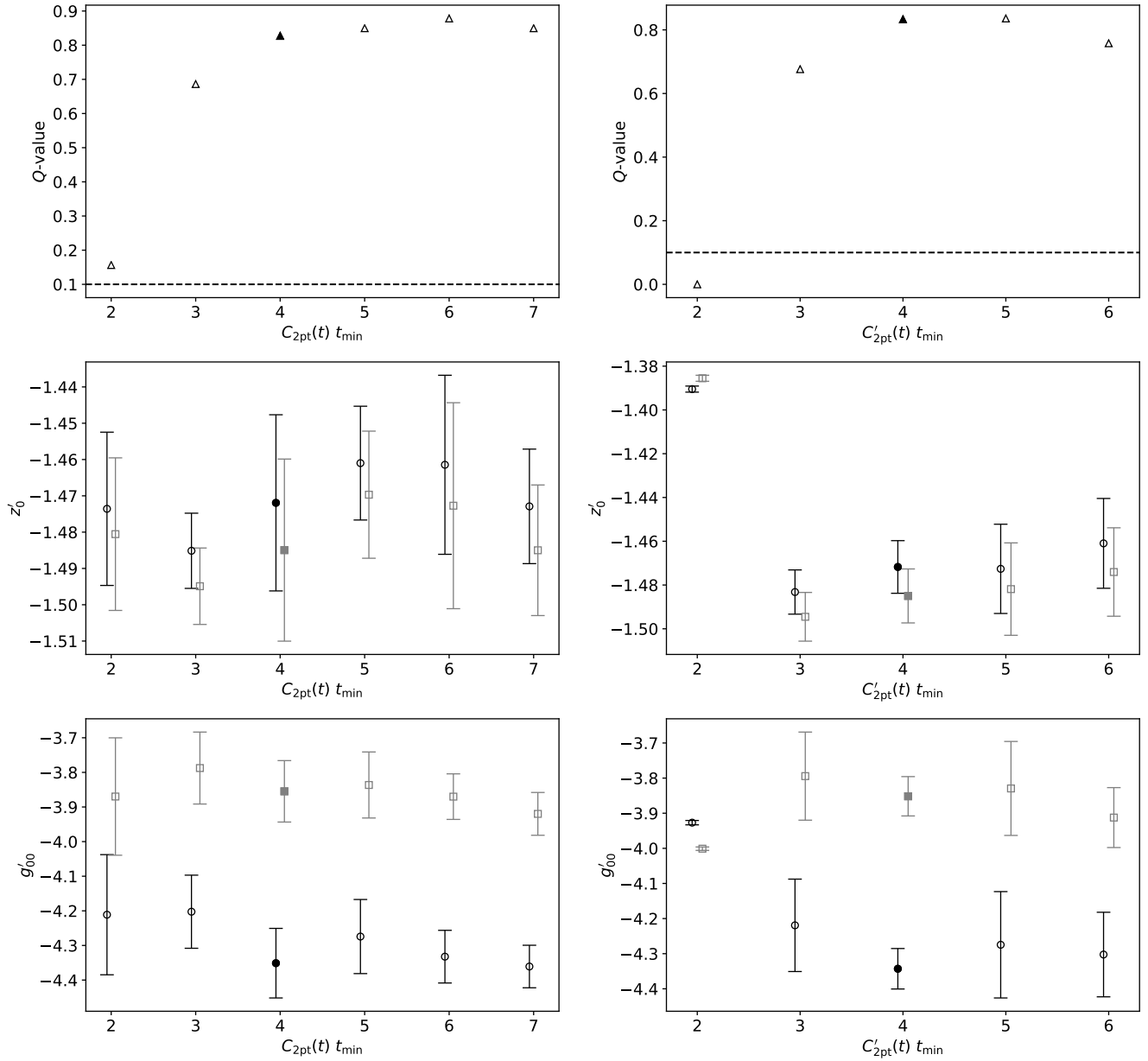**Appendix A: Small volume $t_{\min}$ correlator stability plots**

FIG. 4. Fit sensitivity to variations of $C_{2\mathrm{pt}}(t)$ and $C'_{2\mathrm{pt}}(t)$ fit regions. Shown here are the $t_{\min}$ and n-state stability plots for the Q-value (top row), z'_0 (middle row) and g'_{00} (bottom row). The colors indicate fits with n-state=1 (red), 2 (green), 3 (blue), and 4 (purple). The different momenta are given by k=0 (circle), and k=$2\pi/L$ (square). The preferred fit is denoted by the solid symbol. The dashed line is set to $Q = 0.1$. The $t_{\min}$ values are integer-valued and staggered for visual clarity.
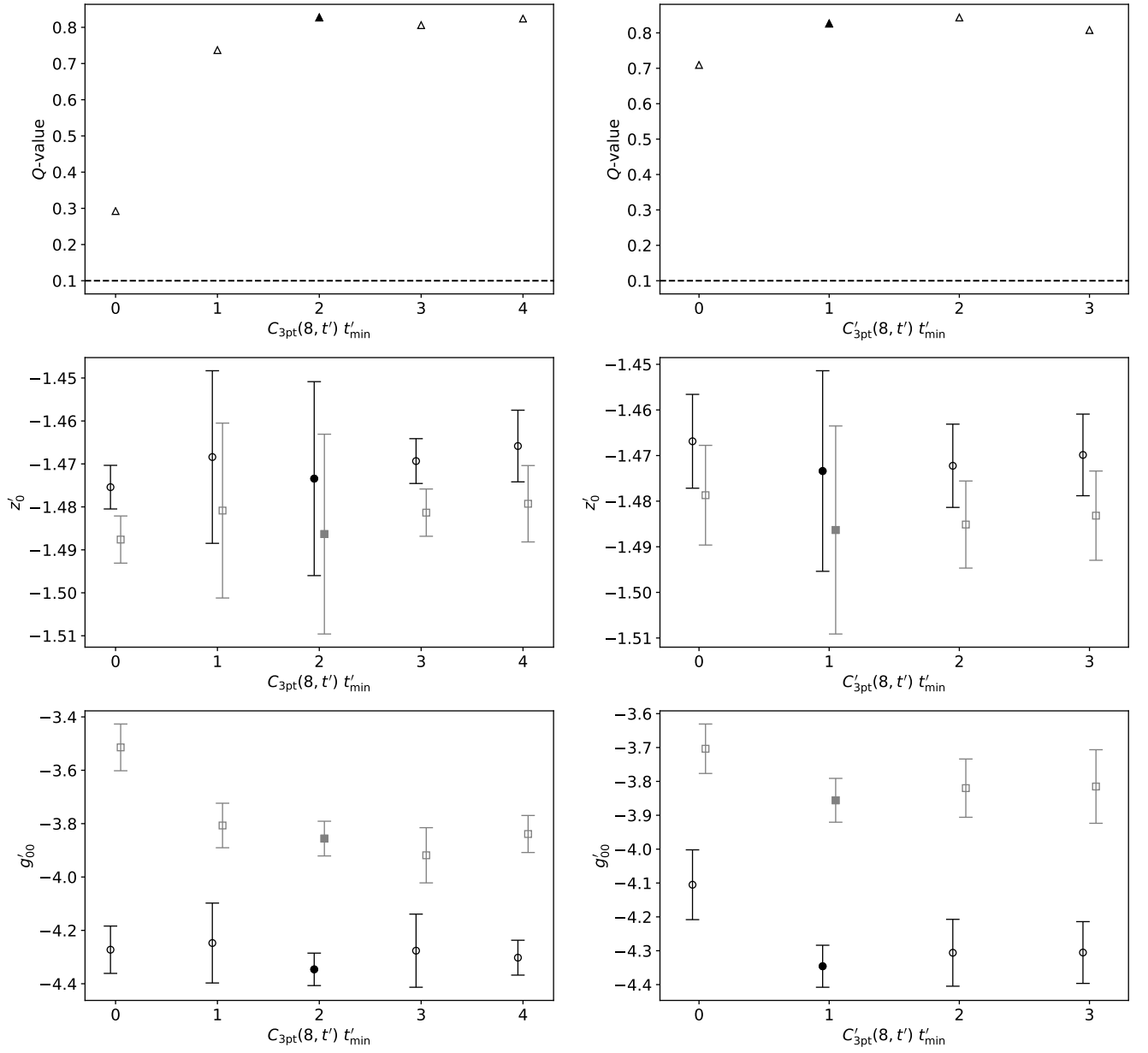
FIG. 5. Fit sensitivity to variations of $C_{3\mathrm{pt}}(8, t')$ and $C'_{3\mathrm{pt}}(8, t')$ fit regions. For $C_{3\mathrm{pt}}$, the data is removed symmetrically around the mid-point. Analogous to Fig. 7.
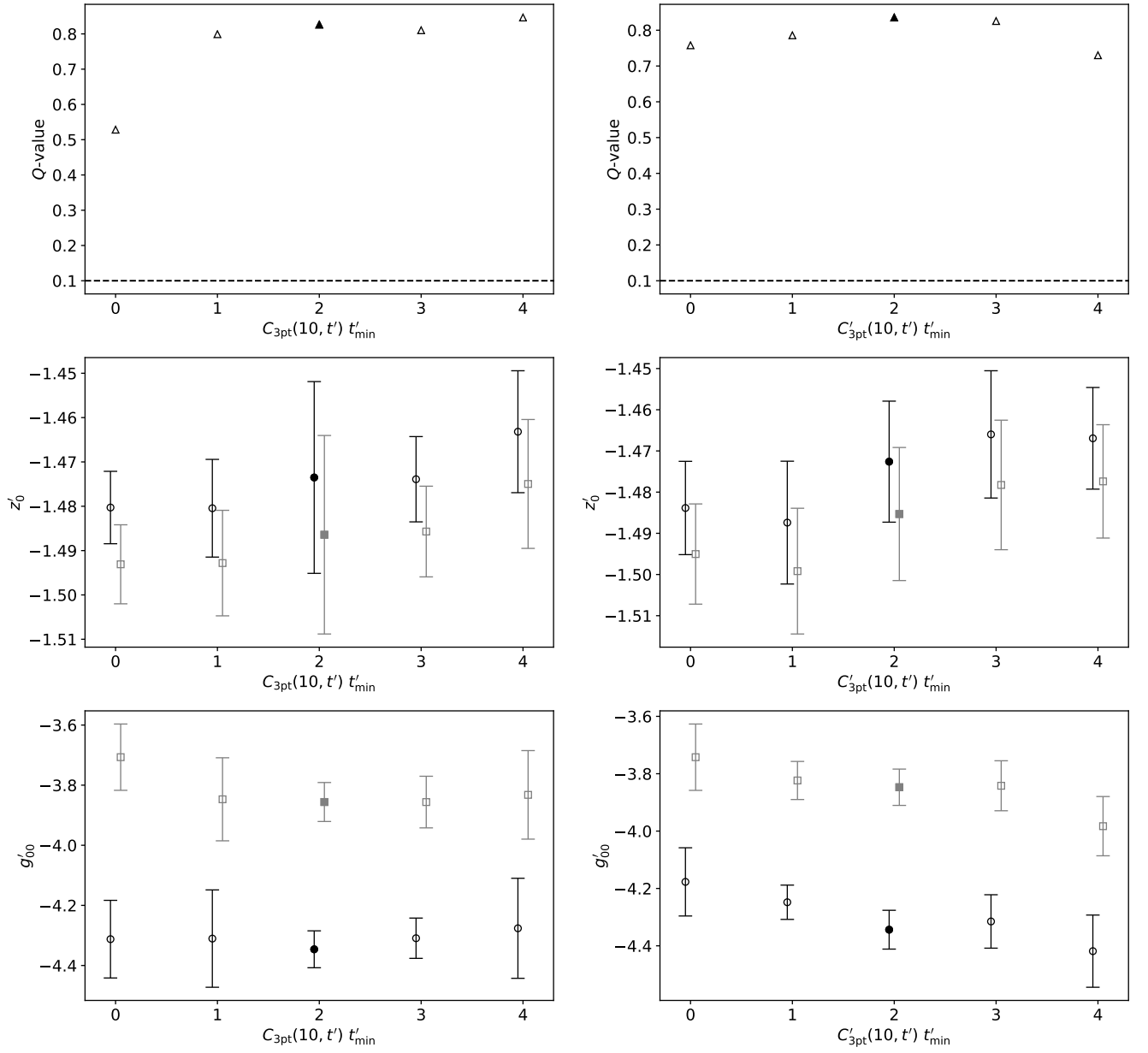
FIG. 6. Fit sensitivity to variations of $C_{3\mathrm{pt}}(10,t')$ and $C'_{3\mathrm{pt}}(10,t')$ fit regions. For $C_{3\mathrm{pt}}$, the data is removed symmetrically around the mid-point. Analogous to Fig. 7.

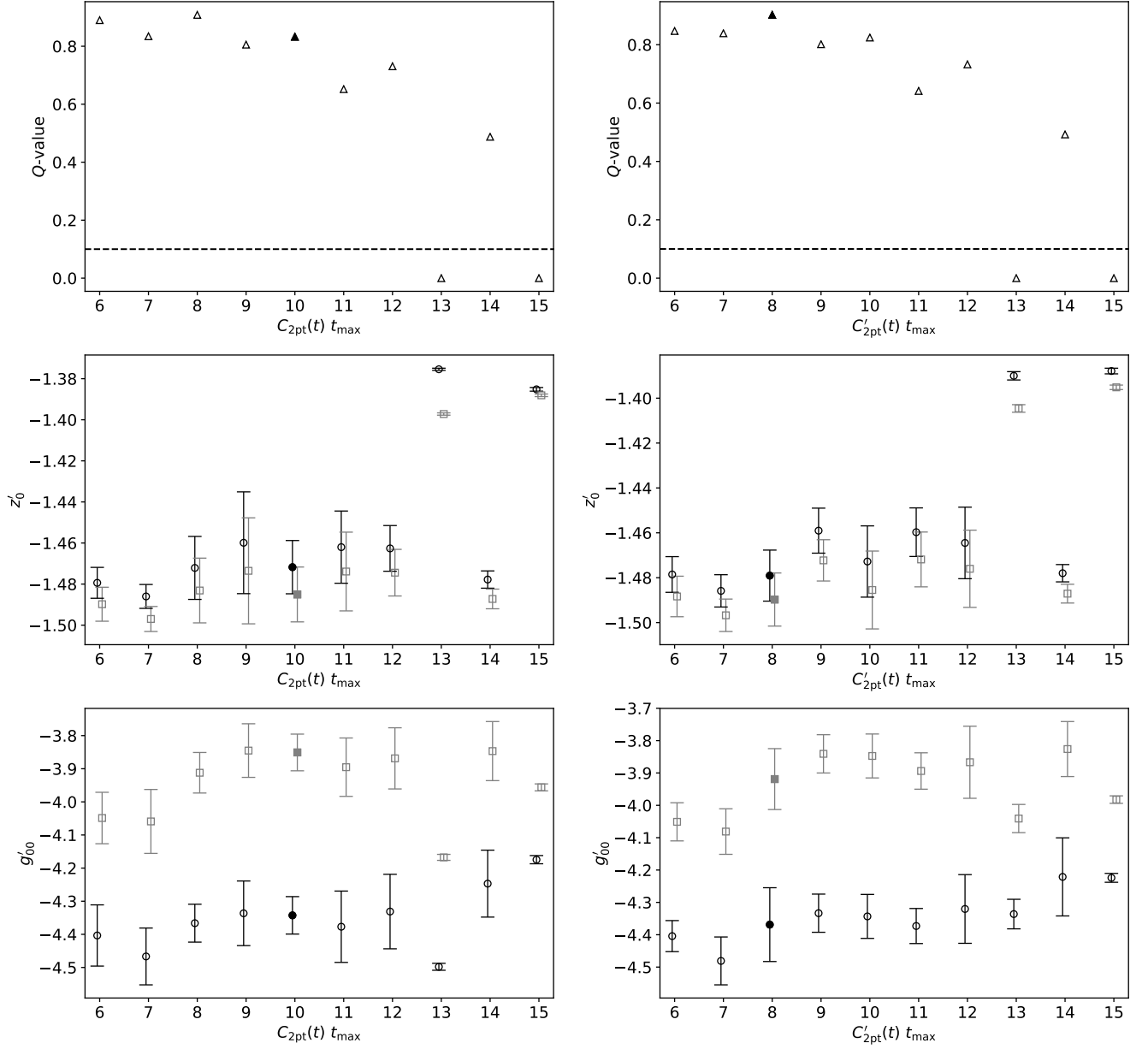**Appendix B: Small volume $t_{\max}$ correlator stability plots**

FIG. 7. Fit sensitivity to variations of $C_{2\mathrm{pt}}(t)$ and $C'_{2\mathrm{pt}}(t)$ fit regions. Shown here are the $t_{\max}$ and n-state stability plots for the Q-value (top row), z'_0 (middle row) and g'_{00} (bottom row). The colors indicate fits with n-state=1 (red), 2 (green), 3 (blue), and 4 (purple). The different momenta are given by k=0 (circle), and k=$2\pi/L$ (square). The preferred fit is denoted by the solid symbol. The dashed line is set to $Q = 0.1$. The $t_{\max}$ values are integer-valued and staggered for visual clarity.
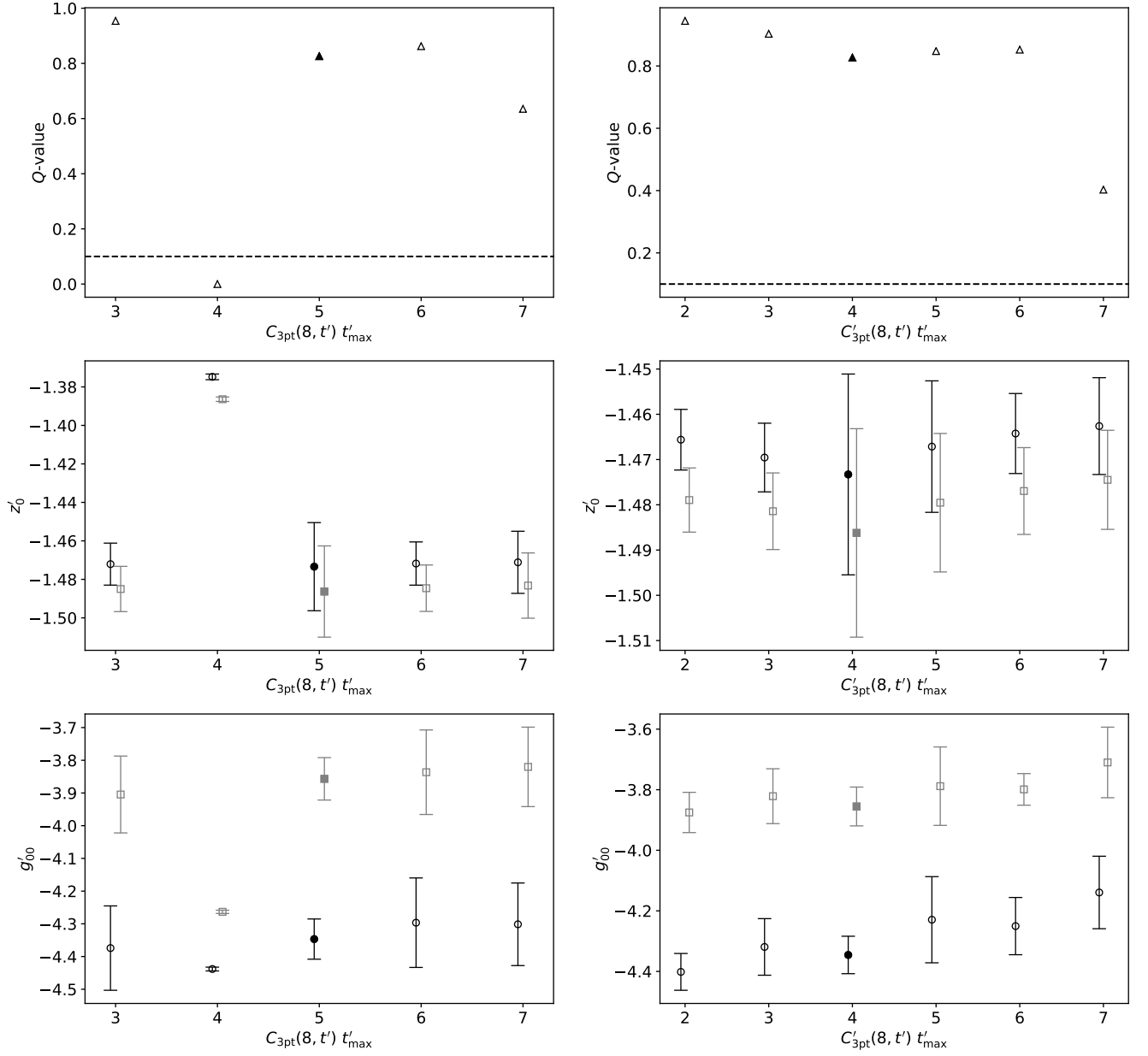
FIG. 8. Fit sensitivity to variations of $C_{3\mathrm{pt}}(8,t')$ and $C'_{3\mathrm{pt}}(8,t')$ fit regions. For $C_{3\mathrm{pt}}$, the data is removed symmetrically around the mid-point. Analogous to Fig. 7.
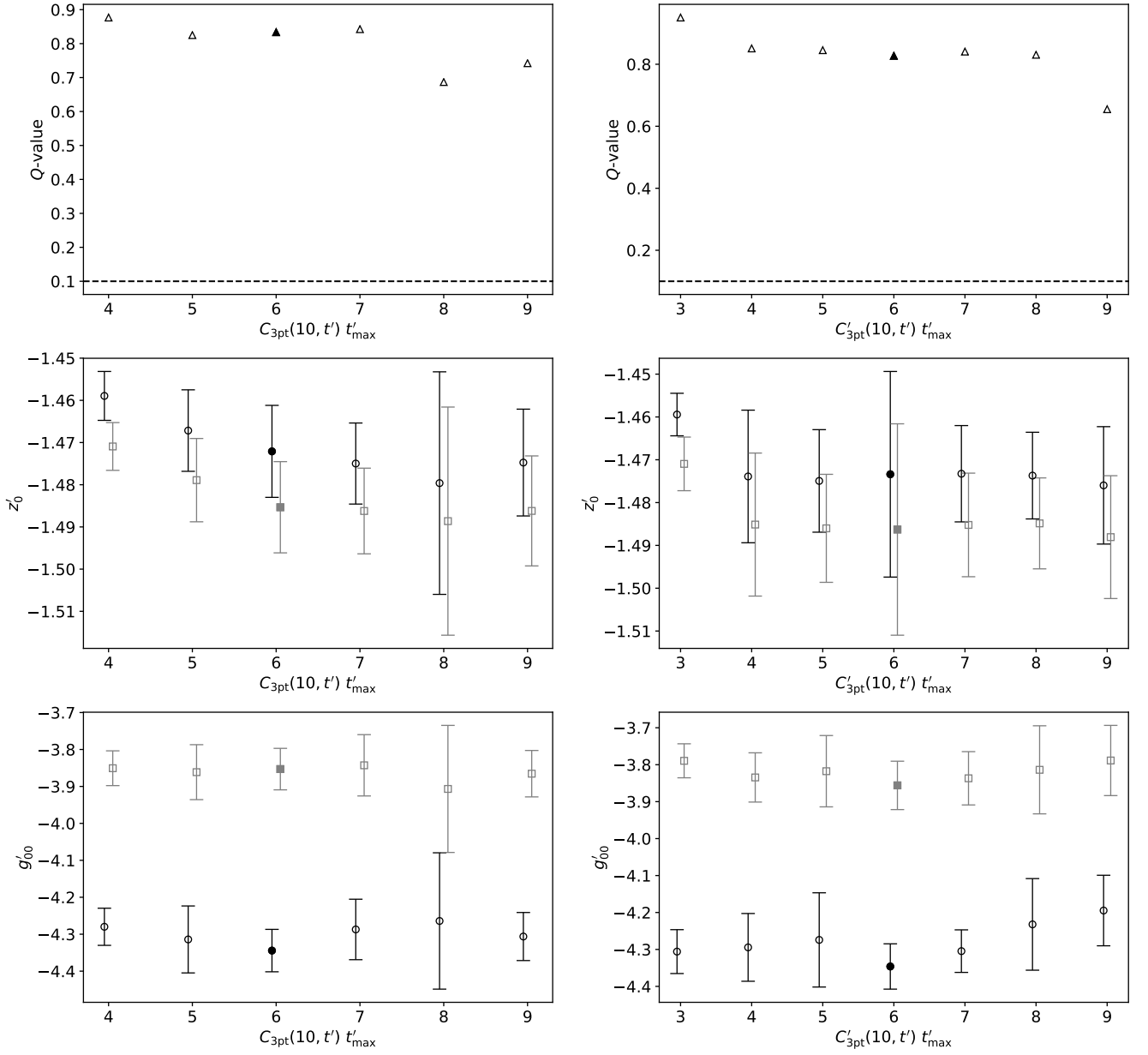
FIG. 9. Fit sensitivity to variations of $C_{3pt}(10, t')$ and $C'_{3pt}(10, t')$ fit regions. For C_{3pt}, the data is removed symmetrically around the mid-point. Analogous to Fig. 7.